Phase Transitions
Publication details, including instructions for authors and subscription information:
http://www.informaworld.com/smpp/title~content=t713647403

Applications in materials science of combining Raman and X-rays at the macro- and micrometric scale

Delphine Vantelon [a]; Pierre Lagarde [a]; Anne Marie Flank [a]; Elise Berrier [b]; Xavier Secordel [b]; Sylvain Cristol [b]; Camille La Fontaine [a]; Françoise Villain [a]; Valérie Briois [a]
[a] Synchrotron SOLEIL, L'Orme des Merisiers, 91192 Gif-sur-Yvette, France [b] UCCS, UMR 8181,Université des Sciences et Technologies de Lille, France

Online Publication Date: 01 April 2009

To cite this Article Vantelon, Delphine, Lagarde, Pierre, Flank, Anne Marie, Berrier, Elise, Secordel, Xavier, Cristol, Sylvain, Fontaine, Camille La, Villain, Françoise and Briois, Valérie(2009)'Applications in materials science of combining Raman and X-rays at the macro- and micrometric scale',Phase Transitions,82:4,322 — 335

To link to this Article: DOI: 10.1080/01411590802655341

URL: http://dx.doi.org/10.1080/01411590802655341

Phase Transitions
Vol. 82, No. 4, April 2009, 322–335

Taylor & Francis
Taylor & Francis Group

Applications in materials science of combining Raman and X-rays at the macro- and micrometric scale

Delphine Vantelon[a], Pierre Lagarde[a], Anne Marie Flank[a], Elise Berrier[b], Xavier Secordel[b], Sylvain Cristol[b], Camille La Fontaine[a], Françoise Villain[a] and Valérie Briois[a]*

[a]*Synchrotron SOLEIL, L'Orme des Merisiers, Saint-Aubin – BP 48, 91192 Gif-sur-Yvette, France;* [b]*UCCS, UMR 8181,Université des Sciences et Technologies de Lille, Bâtiment C3 59655 Villeneuve d'Ascq Cedex, France*

(*Received 7 November 2008; final version received 1 December 2008*)

Simultaneous combination of Raman with X-ray Absorption Spectroscopy (XAS) has become of great interest in Materials Science. Four applications are reviewed in this article that reflect the large range of possibilities offered by such coupling at the macro and micrometer scales. Special emphasis was laid on the macrometer scale on time-resolved studies of physico-chemical transformations, either for providing more complete analysis of structural changes or for looking at the sample integrity. The capability of Raman and XAS to provide complementary chemical and structural information was also pointed out for discriminating and characterizing chemical phases in heterogeneous materials at the micrometer scale.

Keywords: X-ray absorption; X-ray fluorescence; Raman; combination; microbeam

1. Introduction

The use of complementary techniques in Materials Science is a well-established prerequisite to get access to a deep structural description of a given material. Provided that the sample is stable over time or that the sample preparation is fully reproducible, the use of several techniques can be usually carried out separately on the same sample allowing a full description of the system by the assembling of the different results. However in peculiar cases, the simultaneous access to different information on a material by coupling, at the same time on the same sample, complementary techniques is the only way to obtain a unique description of the system and to provide far more details and better understanding on the material than is possible through the juxtaposition of different results issued from separate experiments.

In this general context, an increasing number of publications recently reports the merits and benefits of such powerful approach for the study of materials by Synchrotron Radiation (SR) techniques [1–8]. In this review article, we would like to stress scientifically pertinent for performing such combinations by reporting various examples of combined

*Corresponding author. Email: valerie.briois@synchrotron-soleil.fr

ISSN 0141–1594 print/ISSN 1029–0338 online

DOI: 10.1080/01411590802655341
http://www.informaworld.com

Raman spectroscopy and X-ray Absorption Spectroscopy (XAS) experiments we first carried out at LURE in 2003 [3,4] and now at SOLEIL on different XAS beamlines [7]. These combinations were possible thanks to the development of new performant compact Raman spectrometers equipped with optical fibers which took the measurement capability to the sample rather than requiring the sample to come to the spectrometer. Despite this increased practicability of Raman spectroscopy, implementation of its combination with SR techniques is not straightforward because of the necessity to satisfy technical constraints of both techniques which are sometimes contradictory. For overcoming such difficulty compromises must be found which are, most of the time, at the expense of high quality data recording for at least one of the two photonic probes. Furthermore, the alignment of the two photonic probes on a single sample is tricky and more time consuming than for separate experiments. Thus, the difficulty of such complicated combining set-up must be overcome by real gains on the knowledge of the investigated material. Time-resolved investigations of chemical reactions or studies of materials under external constraint ($T, P, E, \ldots$) and spatially resolved studies of heterogeneous materials are two main and valuable considerations for implementing such combination of techniques. Two examples will illustrate the first point: (i) the kinetic investigation of Ce(IV) reduction in presence of ethanol and (ii) the monitoring of rhenium oxide hydration. Then two spatially resolved experiments at a micrometer scale will be presented: (i) the structural investigation of corrosion products in archeological artefacts and (ii) the study of microcrystalline phases in minerals.

2. Raman methods

The Raman spectra at macro- and micrometer scales were recorded in backscattering geometry with the same Raman spectrometer: a Raman RXN1 analyzer delivered by Kaiser Optical Systems, Inc (KOSI). It incorporates a near-InfraRed laser diode working at 785 nm, a patented HoloPlex transmission grating which diffracts the different wavelengths of the polychromatic Raman scattered light into different angular output paths on the Peltier-cooled Charge Coupled Device detector. This provides a fast and simultaneous full spectral collection of Raman data. Such 'one shot' data acquisition available with this dispersive Raman spectrometer technology provides several advantages for the combination with XAS. This enables a high sampling rate allowing the real-time monitoring of phase modification and the fast acquisition of spatially resolved map. In this later case, due to the minimization of the laser residence at the same point on the sample, the risk of burning the sample by overexposure to the laser is minimized. A laser probe head connected to the spectrometer by two optical fibers is used for delivering the laser on the sample and for collecting the scattered signal. Depending on the investigated system, the probe head can be equipped with noncontact objective lenses with different working distances or with immersion optics. Data over a range from 100 to 3100 cm^{-1} were collected with a resolution of 2 cm^{-1}.

3. Macrometer scale investigation: X-rays methods and materials

The investigation of the reduction of Ce(IV) in presence of ethanol was performed using the synchrotron radiation from the D2 bending magnet of the DCI storage ring (LURE, Orsay, France). Time-resolved X-ray Absorption Near Edge Structures (XANES) data were recorded at the L_3 edge of cerium within a time frame of 5 s for each spectrum using

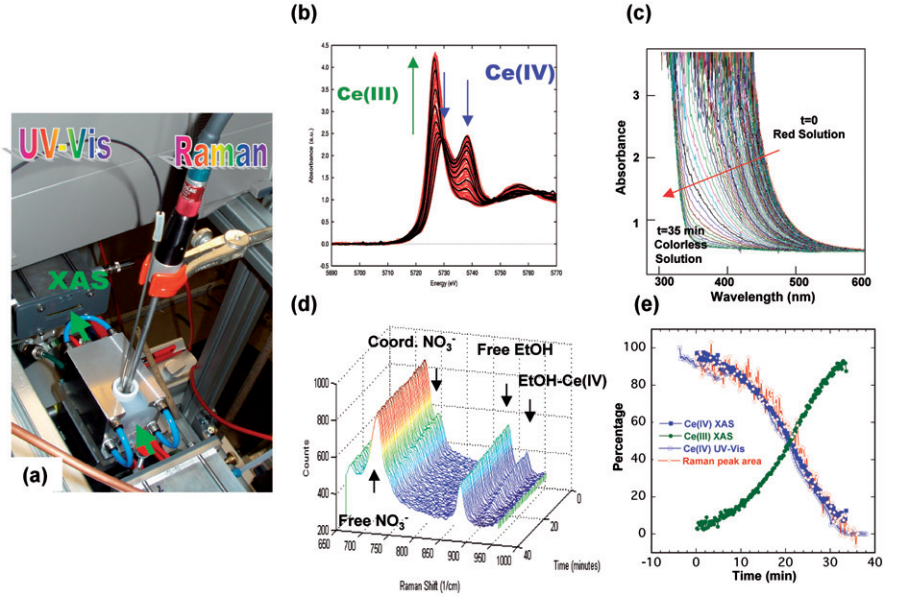

Figure 1. *In-situ* investigation of the kinetic of reduction of Ce(IV) in presence of ethanol using the set-up shown in (a) made of a Kel–F thermostated cell allowing the simultaneous recording of Quick-XANES spectra using the incident and transmitted flux of photons (green arrows) measured by the two ionization chambers, the UV–Vis and Raman spectra using immersion probes in direct contact with the solution through the aperture at the top of the cell; (b) Raw Quick-XANES spectra recorded at the L_3–Ce edge; (c) raw UV–Vis spectra; (d) raw Raman data and (e) profiles of Ce(IV) and Ce(III) percentages in solution determined by Quick-XANES and UV–Vis compared to the profile of intensity of the Raman band at 915 cm^{-1} related to the C–C stretching vibration mode of the ethanol skeleton modified by the complexation with Ce(IV).

the Quick-Extended X-ray Absorption Fine Structure (Quick-EXAFS) monochromator developed by Frahm and coworkers [9]. The time frame for the Raman spectrum collection using the HoloReact software developed by Kaiser is of 13 s, involving 5 s of integration time, cosmic ray detection (5 s) and time for saving the data. Experimental details extensively given in [4] are briefly summarized herein. A thermostated cell maintained at 45°C was filled with a solution containing 2.5 mmol of ceric ammonium nitrate, $(NH_4)_2Ce(NO_3)_6$ in nitric acid and 8.6 mmol of absolute ethanol, CH_3CH_2OH. The cell, presented in Figure 1(a), is equipped with Kapton windows for the collection of Quick-XANES data in transmission mode whereas the aperture at the top of the cell allows for collecting UV–Vis and Raman spectra using immersion probes. The laser power for the experiment was set to 50 mW.

The monitoring of gradual hydration of anhydrous rhenium heptoxide crystal, Re_2O_7, was carried out at SOLEIL on the SAMBA beamline (Spectroscopies Applied to Materials Based on Absorption) [10]. The bending magnet radiation from the SOLEIL source is vertically collimated by a first cylindrical bent mirror onto the Si(111) Fixed Exit Sagitally Focusing Double Crystal monochromator. A second cylindrical bent mirror focuses the monochromatic beam at the sample position onto a spot of $200 \times 300\ \mu m^2$. The X-rays grazing incidence of the mirrors was set at 4 mrad in order to reject harmonics. L_3 Re XAS data were collected in transmission mode using Oxford ionization chambers with a counting time of 1 s and with an energy step of 0.2 eV in the 10515–10575 eV energy range and 0.5 eV at higher energy. In a first experiment, the recording of the data for the

anhydrous Re_2O_7 phase was carried out at 77 K under secondary vacuum using a liquid nitrogen cryostat loaded in a water-free argon atmosphere, thus preventing air–moisture exposition. In a second experiment, the *in situ* RT hydration of a self-supported pellet of anhydrous Re_2O_7 was carried out inside a rectangular aluminium cell in which a stream of He gas containing a few ppm of water flowed. The laser excitation was oriented at 90° with respect to the transmitted X-ray beam whereas the sample orientation was set to 45° with respect to laser and X-rays beam. The Raman probe head equipped of a noncontact long working distance objective (×10) was located outside the sample cell at ~75 mm from the sample. The cell was equipped with Kapton windows (25 μm) for X-rays and Mylar window (50 μm) for Raman. In order to reduce the Raman acquisition time, data were collected without cosmic ray correction with a total integration time of 150 s and the laser power set at 50 mW.

4. Micrometer scale investigation: Materials and X-rays methods

The corroded iron thin section was cut in an iron ingot coming from a roman wreck discovered by A. Chabaud in 1996. The wreck was lying in 12 m of water into the Mediterranean Sea, nearby the Saintes Maries de la Mer (France) [11].

The gneiss thin section was cut in a rock that was collected in the upper part of the Joeri valley (Silvretta mountain area, Switzerland). It was cut and polished to obtain a 90 μm thick, 2 cm large and 3 cm long sample.

The coupling of Raman with X-Ray Fluorescence (XRF) and XAS at the micrometer scale was performed on the LUCIA beamline (located at that time at the Swiss Light Source, Paul Scherrer Institut, Villigen, Switzerland) which is a beamline dedicated to micro X-ray absorption in the tender X-ray domain (0.8–8.0 keV). The beamline set up and capacities are detailed in Flank et al. [12]. Description of the coupling set up and the confocality alignment procedure of X-rays with laser beam are given in Briois et al. [7]. The choice of optics and optical fiber core size used as excitation mainly determined the size of the laser spot at the optimal focus. In both experiments, the same long working distance Olympus lens (×50) is used in conjunction with a single mode optical fiber of 7 μm in diameter. The laser spot size so-obtained is approximately of $5 \times 5\,\mu m^2$ ($H \times V$). All measurements were performed at room temperature, under vacuum (~1 Pa). For the experiment performed at the Fe K edge, XAS scans were recorded using a double crystal Si(111) monochromator with a step size of 0.2 eV and a counting time of 2 s in the XANES region and 2–4 eV and 2–4 s in the Extended X-ray Absorption Fine Structures (EXAFS) region. The X-ray beam size was $15 \times 15\,\mu m^2$ ($H \times V$). For the experiment performed at the Si K edge, XANES spectra were recorded using the double crystal KTP(011) monochromator with a step size of 0.2 eV and a counting time of 2 s. The X-ray beam size was $7 \times 5\,\mu m^2$ ($H \times V$). All measurements were performed collecting the fluorescence (FY) signals from the samples using a single-element silicon drift detector. Fluorescence signals were corrected from the dead time of the fluorescence detector, and from self-absorption using the Athena software [13] assuming the elemental composition of the identified phase and the following experimental configuration: the sample holder was oriented perpendicular to the incident beam and the fluorescence signal was recorded with an exit angle of 17° to the surface. XANES normalization and EXAFS extraction were done using the Athena software [13]. Fe K edge EXAFS spectra were fitted using FEFF7 under the Artemis software [13] considering in the single scattering approximation the atacamite structure model [14] in which Cu is replaced by Fe. Simultaneously to the μ-XRF mapping

on a selected region of the corroded iron ingot section, μ-Raman mapping of the same region was carried out. The recording of the Raman signal was triggered by the Multi Channel Card used for the μ-XRF acquisition. The integration time in each point of the Raman and XRF maps recorded simultaneously was 20 s.

5. Results and discussion

5.1. *Macrometer scale investigations*

Two examples of time-resolved investigations of phase transformations are first presented as typical examples of combination of Raman with XAS at a macrometer scale.

The first example related to the study of the reduction of ceric cations by ethanol illustrates the potentiality offered by such combination for accessing to unique complementary time-resolved information related to the metallic element target with XAS and to the ligands coordinated to the metal with Raman spectroscopy [4].

The reaction was investigated simultaneously by Quick-XANES at the L_3 Ce edge and UV–Vis and Raman spectroscopies. Figure 1(b)–(e) presents the results so-obtained.

X-ray Absorption Spectroscopy data (Figure 1b) allows the quantification of Ce(IV) and Ce(III) species in solution. Indeed the reduction of ceric cations gives rise to a continuous modification of XANES shape which results from the continuous change in solution of the proportion of Ce(III) and Ce(IV) ions. The measured spectra at any stage of the reduction can be rebuilt using a linear combination of the extreme spectra of the reaction, i.e., the spectrum recorded at $t = 0$ and the one recorded at the end of reduction, allowing the determination of proportions of Ce(IV) and Ce(III) in solution.

Macroscopically the addition of ethanol to a solution of Ce(IV) immediately gives rise to a color change of the solution from yellowish to red. This behavior is due to the formation of a complex between the cerium ion and ethanol. Then the red solution progressively turns into a colorless solution due to the slow reduction of cerium (IV) into cerium (III) and then concomitant oxidation of ethanol. Such color change is well-characterized by UV–Vis spectroscopy which presents a continuous shift of the absorption threshold from 460 to 310 nm (Figure 1c). The complete reduction of Ce(IV) into Ce(III) in presence of excess of absolute ethanol takes place in ~35 min at the reaction temperature. Using the relationship between the measured absorbance and the concentration of Ce(IV), which is the only colored species in solution ($\text{Absorbance}(t) = \varepsilon l[\text{Ce(IV)}]_t$), UV–Vis data can be also used to determine the concentration of Ce(IV) cations in the media.

Besides Raman spectroscopy presented in Figure 1(d) clearly evidences the formation of the complex between Ce(IV) and ethanol with the appearance of a new band in the region of the C–C stretching mode of ethanol located at 915 cm^{-1} at the right side of the band at 880 cm^{-1} due to free ethanol. Additionally the analysis of the υ_4 vibration mode of nitrate species in the 700–750 cm^{-1} range shows that a part of nitrate is coordinated to the cerium. Finally, the close inspection of the time-resolved evolution of the Raman data also evidences that the complex between Ce(IV) and ethanol and the bond between nitrate and Ce(IV) both disappear upon ethanol oxidation.

Finally, the consistency of the approach used in the investigation of the reduction kinetic is illustrated in Figure 1(e) by the comparison of the profile of ceric and cerous species concentrations coming from the UV–Vis and XAS spectroscopies together with the time evolution of the integrated area of the Raman band which characterizes the

complexation of Ce(IV) either with nitrate or with ethanol. The results reported herein with the combination of techniques clearly indicate that no intermediate species in the reduction of cerium (IV) by ethanol is formed.

It is noteworthy that the complementary information available using the Raman spectroscopy, in particular the information dealing with the coordination of Ce(IV) by nitrate ligands, was very important to improve the fit of the EXAFS data recorded for the two species in presence during the reaction. Namely, it is known from Raman that nitrate is coordinated to the cerium in the initial Ce(IV) species. Such information can be rightly used in the EXAFS simulation of the ceric species by introducing in the structural model nitrate ligands to simulate atomic contributions beyond the first coordination shell. This point is discussed in details in reference [4].

Beyond the complementary information available with the combination of techniques, this example illustrates as well how such combination of Raman with XAS can give more reliability to the interpretation of results gained by one of the two techniques. Here Raman spectroscopy gave hints for analyzing second coordination shell around Ce, and reciprocally the discrimination between different backscatters possible by EXAFS could be fruitful for identifying vibration modes of the Raman data.

The second example illustrates the potentiality offered by the combination of techniques to investigate the integrity of the sample during its characterization. Thus, Raman spectroscopy was used to both check the structure of the starting material and monitor the structural changes occurring upon a controlled hydration of the solid. The very broad field of applications of this oxide in catalysis and the lack of due spectroscopic investigation on such rhenium compounds motivate this rather fundamental study which consists in associating unambiguously the XAS spectrum to a known chemical species simultaneously monitored by Raman spectroscopy. Besides the number of reported XAS data recorded at the L_3 Re edge is rather scarce in the literature and the set of data recorded using the combination of Raman will serve as data bank in forthcoming *operando* studies of supported rhenium oxides used as selective catalysts for methanol oxidation reactions [15].

Figure 2 displays the Raman spectrum of anhydrous Re_2O_7 recorded at 77 K in the hermetic cell maintained under secondary vacuum, whereas Figure 3(a) depicts Raman data collected during the controlled hydration of Re_2O_7 by a slightly wet helium flow.

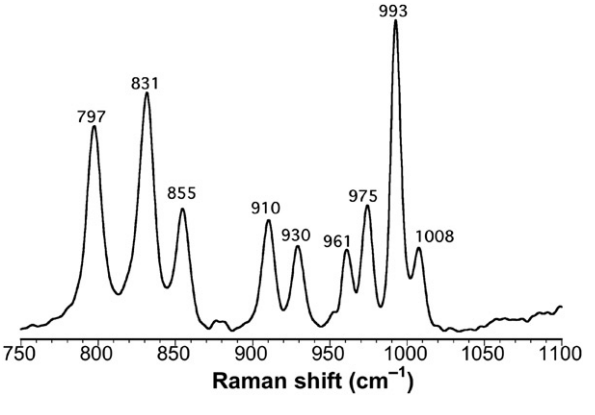

Figure 2. Raman spectrum recorded for anhydrous Re_2O_7, this spectrum has been recorded simultaneously with the XANES spectrum displayed in Figure 3(b).

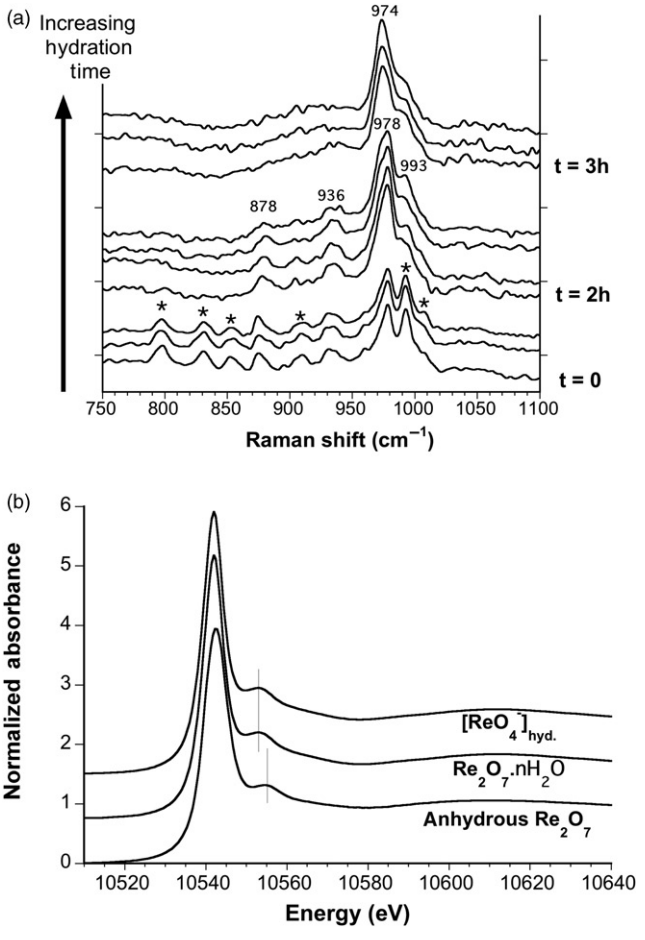

Figure 3. (a) Raman data collected during the controlled hydration of anhydrous Re_2O_7; (b) normalized L_3–Re edge XANES spectra recorded for the anhydrous Re_2O_7 crystal, during the period $t = 120$–180 min of hydration corresponding to the hydrate $Re_2O_7 \cdot nH_2O$ crystal, and after 200 min of hydration corresponding to the hydrated $[ReO_4^-]$ species.

Solid Re_2O_7 is very sensitive to air–moisture exposure so that the transfer operation in glove box and sealed spectroscopic cell for this second experiment led to a certain hydration at $t = 0$. Indeed, the first Raman spectrum in Figure 3(a) is clearly a linear combination of the Raman features of anhydrous Re_2O_7 crystal already presented in Figure 2 and for which the more intense bands are marked by a star together with new sharp Raman lines at 878 and 978 cm^{-1} assigned to a partially hydrated, well-crystallized solid labelled hereafter $Re_2O_7 \cdot nH_2O$. Both Re_2O_7 and $Re_2O_7 \cdot nH_2O$ species coexist during the first 2 h of controlled hydration. Then, the hydrated crystal, $Re_2O_7 \cdot nH_2O$, is the only rhenium component in the pellet and remains stable for 1 h of subsequent hydration. Finally after a total of 3 h of exposure to the He/H_2O gas stream, the presence of an intense single peak at 974 cm^{-1} overlapping with a shoulder at 920 cm^{-1} is characteristic of the presence of ReO_4^- perrhenate anion. Details about the Raman band assignations will be given in a forthcoming publication [15]. Such monitoring by Raman of the hydration steps of the dirhenium heptoxide allows us to

start the XANES acquisition for the $Re_2O_7{\cdot}nH_2O$ and $HReO_{4(hydrated)}$ species at the right period, that means when these species are the only stable species in presence. In this way, the normalized L_3-Re edge of the three hydration stages of dirhenium heptoxide, namely anhydrous Re_2O_7, $Re_2O_7 \cdot nH_2O$ and fully hydrated $ReO_{4\,(hydrated)}^{-}$ species, which are all positively identified at once by Raman spectroscopy, are presented in Figure 3(b). Such identification is mandatory when a compound is likely to be subjected to structural changes, so far as the modifications of the XANES shape are very faint and denote very subtle structural differences as shown in Figure 3(b). Namely, the anhydrous dirhenium heptoxide is described as a polymeric solid state structure of strongly distorted ReO_6 octahedra and fairly regular ReO_4 tetrahedra [16] sharing one oxygen atom, whereas the hydrate $Re_2O_7{\cdot}nH_2O$ with $n=2$ consists of an almost undistorted ReO_4 tetrahedron sharing one oxygen atom with a distorted octahedron around Re [17] involving water molecules at an average distance $\sim$0.5 Å longer than the other nonbridging Re–O distances. As expected considering these structural descriptions, the difference between the L_3 XANES spectra of Re_2O_7 and $Re_2O_7 \cdot nH_2O$ species is mainly evident in the region of the absorption spectrum sensitive to multiple scattering processes of the photoelectron beyond the first coordination shell, i.e., just above the intense white line. It is noteworthy that the marked increase of the intensity of the white line upon hydration of the dirhenium heptoxide crystal reflects an increase of vacant density of 5d states resulting from the breaking of the polymeric structure and substitution of strongly covalent oxo ligands by less covalent water molecules. Finally, no difference between the XANES spectra of $Re_2O_7 \cdot nH_2O$ and fully hydrated $ReO_{4\,(hydrated)}^{-}$ species is evident. This suggests that the hydrate and fully hydrated species are from a local point of view structurally much closer than it could be expected from the crystallographic structure description. We should stress here that the only way to distinguish between these two hydrates of rhenium heptoxide, if they appear as results of a catalytic reaction investigated by XAS, is to use the Raman spectroscopy as complementary analytical tool since both species present close but nevertheless distinct Raman features.

This second example illustrates well how powerful the combination of Raman and XAS spectroscopies is for detecting on purpose or accidentally physico-chemical changes of the sample during data recording. Without this combination, it would have been impossible to definitely connect the recorded XANES structures and the different stages of Re_2O_7 hydration and to have information on 'what we were looking at.' The combination is of peculiar relevance in the present case since the hydration process is featured by small changes in the XANES spectra compared to the anhydrous state and by no change considering the two hydrate forms of the rhenium heptoxide. Such monitoring by Raman spectroscopy of the good 'health' of the sample is important for air or water sensitive samples, and particularly crucial for Synchrotron Radiation investigations using very intense X-rays beams delivered by third generation sources often responsible for radiation damages [18].

5.2. *Micrometer scale investigations*

Coupling two structural and local techniques, with microanalysis capabilities, is of major importance in the study of very poorly defined heterogeneous materials like corrosion layers, soils or rocks since very different types of chemical species can coexist at a scale of a few micrometers.

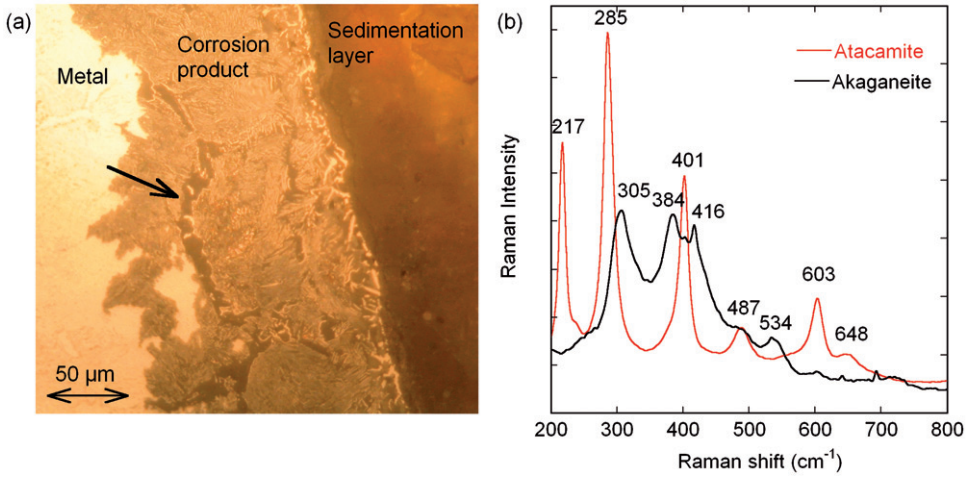

Figure 4. (a) Optical microscope image of the studied thin section. Three areas are distinguishable: the unaltered metal in light brown on the left of the image, the sedimentation layer in dark brown on the right of the image that corresponds to a zone of precipitated materials from sea water, and in between, the heterogeneous area of the corrosion products where cementite, akaganeite, and ferrous hydroxychloride were identified. The area mapped in XRF and Raman is pointed out by the arrow; (b) Raman spectra of akaganeite and atacamite.

The first example of application takes place in the context of the optimization of iron artefacts dechloration. Indeed, remains of chlorine in the corrosion crust of iron objects are responsible for their alteration after excavation. Among the corrosion products of iron archeological materials in marine environment, two chlorinated species were identified: the well-known akaganeite and a second species recently discovered and not yet fully characterized. It was proposed to call it ferrous hydroxychloride [$Fe(II)_2(OH)_3Cl$] since it exhibits a higher content in chlorine than akaganeite (15–20% mass *vs.* 5–8%) and its Raman spectrum and XRD diffractogram present similarities with those of atacamite [$\beta Cu_2(OH)_3Cl$] [19,20]. Additional EXAFS experiments would give information on the local order of this structure. Unfortunately, this phase is unstable when synthesized. Thus it is necessary to study the natural phase *in situ* despite it occurs as a minor phase among the iron corrosion products that are forming a corrosion crust 50–100 µm thick. In these conditions, working on thin section samples using a microbeam appears to be necessary to single out the given species and study the eventual spatial variations of the structure. Combination with µ-Raman appears essential to rapidly localize the given species and confirm the spectrum assignment.

Figure 4(a) shows an image by optical microscope of the studied thin section in which the area mapped simultaneously by XRF and Raman is pointed out by the arrow. Previous Raman analyses (D. Neff, lab. P. Sue) revealed presence of cementite (Fe_3C, 0% Cl), akaganeite (βFeOOH, 5–8% Cl) and ferrous hydroxychloride [$Fe(II)_2(OH)_3Cl$, 15–20% Cl] in the corroded area. Raman spectra of akaganeite and atacamite are reported in Figure 4(b) (Cementite is Raman inactive). The characteristic band of atacamite at 603 cm^{-1} is shifted to 618 cm^{-1} in the ferrous hydroxychloride phase [19] which corresponds to a nearly silent region for akaganeite under 785 nm laser excitation. The integrated intensity of the 618 cm^{-1} band was selected for the collection of the Raman map displayed in Figure 5(a). XRF maps of the Fe and Cl Kα

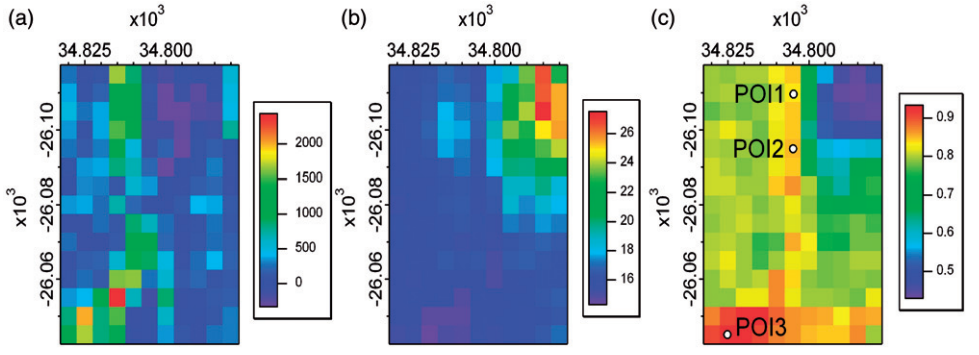

Figure 5. Maps $50 \times 70\,\mu m^2$, 5 µm steps, counting time 25 s for XRF and 1 s for Raman; (a) Intensity of the Raman band at $618\,cm^{-1}$ [characteristic of β-$Fe_2(OH)_3Cl$]; (b) and (c) intensity of the Kα fluorescence peaks collected at the incident energy of 7.2 keV for, respectively, Fe and Cl.

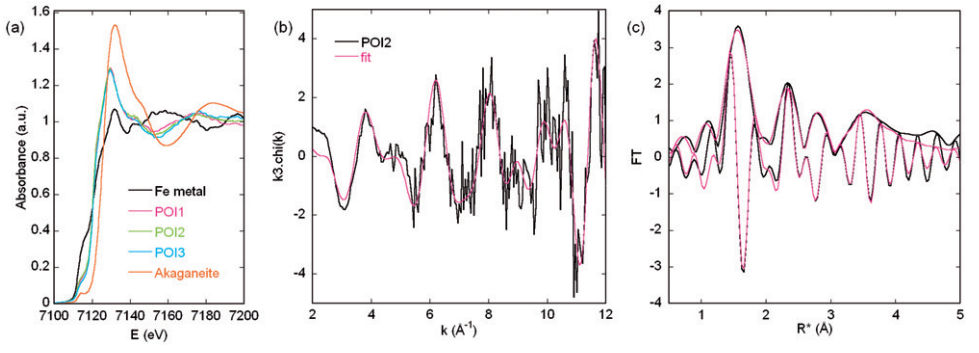

Figure 6. (a) XANES spectra collected at the Fe K edge in the zone enriched in Cl (POI 1 POI 2 and POI 3) and metal iron and akaganeite as references; (b) EXAFS spectra, and (c) corresponding Fourier transform (amplitude and imaginary part) collected in POI 2. Fit is reported in pink.

line intensity are reported in Figure 5(b) and (c). XANES and EXAFS spectra collected in several points of interests (POIs) are reported in Figure 6. POIs location is reported on Figure 5(c).

The Fe map (Figure 5b) does not show any precise location of the ferrous hydroxychloride species while Cl map (Figure 5c) evidences a thin long zone in the center of the map with a slightly increased content in Cl. This increase is correlated with a significant increase of the Raman band at $618\,cm^{-1}$ (Figure 5a).

XANES spectra taken in various POIs in the zone are all similar. They exhibit a pre-edge at 7113 eV and an edge at 7120 eV. The white line maximum is at 7129.4 eV with a shoulder at 7142 eV. A broad oscillation occurs at 7174 eV. According to the edge position, which is in between metal Fe [Fe(0)] and akaganeite [Fe(III)], the degree of oxidation of iron is 2+, in agreement with the hypothesis of ferrous hydroxychloride phase. Results of the simulation of the EXAFS signal recorded for one of the POIs discriminated by Raman as characteristic of the ferrous hydroxychloride phase are gathered in Table 1 and compared to the radial distributions of atoms around the two sites of copper in the atacamite structure. The octahedrons of the first copper

Table 1. Simulation results of the EXAFS signal collected in POI compared to the atomic distances in the atacamite mineral.

	Atacamite (from [14])	
Ferrous hydroxychloride EXAFS simulation	Site 1	Site 2
	First shell	
4 O at 2.02 Å	2 O at 1.94 Å	2 O at 1.99 Å
Sigma2 = 0.0013 Å^2	2 O at 2.02 Å	2 O at 2.01 Å
2 Cl at 2.73 Å	2 Cl at 2.78 Å	1 O at 2.36 Å
sigma2 = 0.0022 Å^2		1 Cl at 2.75 Å
	Second shell	
2 Fe at 3.16 Å	2 Cu at 3.11 Å	2 Cu at 3.02 Å
Sigma2 = 0.0041 Å^2	2 Cu at 3.38 Å	2 Cu at 3.11 Å
4 Fe at 3.72 Å	2 Cu at 3.43 Å	2 Cu at 3.38 Å
Sigma2 = 0.0020 Å^2	2 Cl at 4.43 Å	1 Cl at 3.95 Å
6 Cl at 4.01 Å		2 Cl at 4.01 Å
Sigma2 = 0.0028 Å^2		1 Cl at 4.33 Å
		2 Cl at 4.35 Å

site in atacamite form chains linked by edges O–Cl whereas the octahedrons of the second copper site connect these chains by two times double-edges bounds, O–O–O and O–Cl–O.

Simulations were performed keeping the Debye–Waller factors of all paths as homogeneous as possible. First of all, chlorine neighbors are found in the first and second coordination shells of iron but as expected when replacing Cu by Fe, some distortions occur evidenced by the slightly smaller Fe–Cl distances than Cu–Cl ones (Table 1). Distortion of the structure is also visible for the Fe–Fe distances. The contribution of Fe neighbors was simulated using two distances, the shortest one for the Cu paths at 3.02 and 3.11 Å and the longest one for the Cu paths at 3.38 and 3.43 Å. The simulation evidences longer Fe–Fe distances showing one at 3.17Å, slightly longer than 3.11Å, and the second at 3.73Å, strongly longer than 3.43Å. Thus, despite small variations, at a really short distance, the overall structure determined by the fit is in satisfactory agreement with the atacamite one confirming the Raman and XRD preliminary results. Further analyses are in progress to fully characterize this phase in the context of the ODEFA PNRC research program.

This example illustrates how the combination of μ-Raman spectroscopy can be helpful for better discriminating chemical phases with close elemental composition within element specific μ-XRF mapping. Then beamtime can be saved for more time consuming experiments, like recording high quality EXAFS data.

The second example of application illustrates the potential of the additional information that can be provided using the polarization of the beam.

Results shown in Figure 7 were obtained from a thin section of a gneiss rock. The elements of interest are aluminium and silicon, which are the major elements of the minerals forming gneiss that are quartz, feldspar and mica. Figure 7(a) and (b) shows a mapping of aluminium and silicon for the same zone of the sample. A Point of Interest (POI) was selected at the border of an isolated region around 30 μm wide where XANES spectra at the silicon K edge were recorded, together with a Raman spectrum.

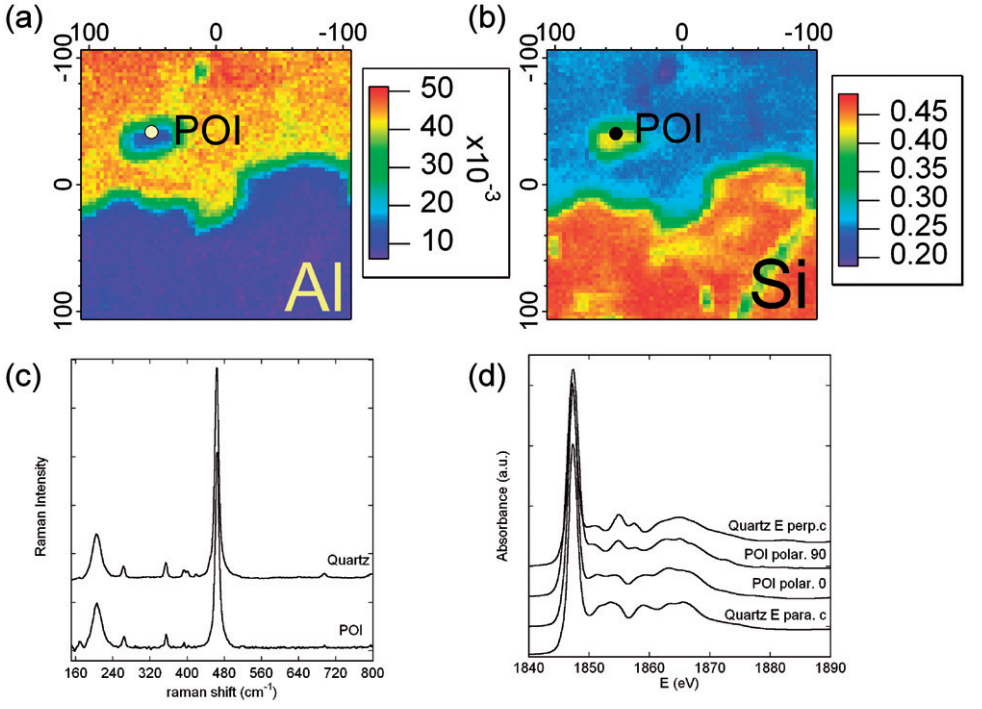

Figure 7. XRF maps of (a) Al and (b) Si collected at 1900 eV. Map size is $210 \times 210\,\mu m^2$, collected with steps of $3 \times 3\,\mu m^2$ and 1 s dwell time. A spot (POI) was selected in the area where silicon appears as main element; (c) The Raman spectrum identifies the species as pure quartz; (d) The Si K edge XANES spectra collected in 0° and 90° polarization are identical to those previously published [21].

The resulting spectra are gathered, respectively, in Figure 7(c) and (d) where relevant reference spectra are also shown.

X-Ray Fluorescence recorded at this POI shows mostly Si with a small contribution from Al. The Raman spectrum (Figure 7c) is characteristic of the α-SiO_2 quartz phase, with no evidence of another phase. Aluminium, revealed by XRF, is then probably involved in a compound much less Raman-active than α-SiO_2 and/or in a so-small quantity that cannot be detected by Raman. The silicon XANES spectrum (Figure 7d) presents some similarities with that of quartz powder, but rather seems to be almost identical to that of pure quartz with its *c*-axis oriented along the photon electric field. In order to confirm this interpretation, we have collected the same spectrum on the same spot after setting the Apple-II undulator polarization to vertical. This ability of the insertion device allows for changing the X-ray beam polarization on the sample without moving it. The two spectra are fully in line with the experimental polarized data obtained with a macrobeam on an oriented single-crystal of quartz and modelled by full multiple scattering calculations [21].

This example illustrates the benefit of combining polarized XAS experiments with nonpolarized Raman spectroscopy. Indeed, as most of the XAS data are recorded for powders, it is not obvious to identify microcrystalline phases just by looking at its polarized XAS spectra. Then the chemical species identification using Raman spectra library can be sometimes unique for detecting polarization effects on XAS spectra of

microcrystalline phases. In several cases, the reactivity of a solid depends upon the crystallographic plane exposed to the reactants and this behavior can be of a fundamental importance in the studies of pollution processes of soils, in which reactive minerals are often microcrystallized. Polarized micro-XAS experiments, which now can be easily and rapidly recorded at the micrometer scale by tuning the insertion device, give a set of complementary information. Thus, a micro-sample can be described beyond its crystallographic nature.

6. Conclusions

An immense step forward in the characterization of Materials has been done with the recent development of simultaneous combination of Raman with SR techniques, which provides a more complete analysis of samples. This article examines the benefits offered by the combination of Raman with X-ray absorption spectroscopy through the presentation of four nonexhaustive applications at the macro- and micrometer scales. Nowadays the combination is clearly beyond the state of proof of principle and its impact in solving questions in many scientific domains does not have to be demonstrated anymore. Despite its complexity, such combination of nontrivial techniques should become commonly available for the users of synchrotron radiation facilities.

Acknowledgements

C. L. F. acknowledges financial support by the Agence Nationale pour la Recherche (ANR-SAXO). Part of this work has been performed at the Swiss Light Source, Paul Scherrer Institut, Villigen, Switzerland. We are grateful to the machine and beamline groups whose outstanding efforts have made these experiments possible. We also thank Dr. A. Hofmann (Univ. Lille) for providing the thin section rock sample, Dr. D. Neff (Lab. P. Sue, CEA) for providing the iron ingot thin section prepared in the context of the ODEFA PNRC research program, Dr. S. Reguer for providing the akaganeite reference and S. Legros (CIRAD, La Réunion) for providing the atacamite one.

References

[1] G.K. Bryant, H.F. Gleeson, A.J. Ryan, J.P.A. Fairclough, D. Bogg, J.G.P. Goossens, and W. Bras, *Raman spectroscopy combined with small angle x-ray scattering and wide angle x-ray scattering as a tool for the study of phase transitions in polymers*, Rev. Sc. Inst. 68 (1998), pp. 2114–2117.

[2] S. Ran, D. Fang, I. Sics, S. Toki, and B.S. Hsiao, *Combined techniques of Raman spectroscopy and synchrotron two-dimensional x-ray diffraction for in-situ study of anisotropic system: Example of polymer fibers under deformation*, Rev. Sc. Inst. 74 (2003), pp. 3087–3092.

[3] V. Briois, S. Belin, F. Villain, F. Bouamrane, H. Lucas, R. Lescouëzec, M. Julve, M. Verdaguer, M.S. Tokumoto, C.V. Santilli, S.H. Pulcinelli, X. Carrier, J.M. Krafft, C. Jubin, and M. Che, *New insights for Materials Science Characterisation using different complementary techniques combined with X-ray Absorption Spectroscopy*, Phys. Scrypta T115 (2005), pp. 38–44.

[4] V. Briois, D. Lützenkirchen-Hecht, F. Villain, E. Fonda, S. Belin, B. Griesebock, and R. Frahm, *Time-resolved study of the oxidation of ethanol by Cerium IV using combined Quick-XANES, UV-Vis and Raman spectroscopies*, J. Phys. Chem. A 109 (2005), pp. 320–329.

[5] A.M. Beale, A.M.J. van der Eerden, K. Kervinen, M.A. Newton, and B.M. Weckhuysen, *Adding a third dimension to operando spectroscopy: a combined UV–Vis, Raman and XAFS setup to study heterogeneous catalysts under working conditions*, Chem. Commun. (2005), pp. 3015–3017.

[6] R.J. Davies, M. Burghammer, and C. Riekel, *Simultaneous μ Raman and synchrotron radiation microdiffraction: Tools for materials characterization*, Appl. Phys. Lett. 87 (2005), pp. 264105-1–264105-3.

[7] V. Briois, D. Vantelon, F. Villain, B. Couzinet, A.M. Flank, and P. Lagarde, *Combining two structural techniques at the micrometer scale: μ-XAS and μ-Raman spectroscopies*, J. Synch. Rad. 14 (2007), pp. 403–408.

[8] E. Boccaleri, F. Carniato, G. Croce, D. Viterbo, W. Van Beek, H. Emerich, and M. Milanesio, *In situ simultaneous Raman/high-resolution X-ray powder diffraction study of transformations occurring in materials at non-ambient conditions*, J. Appl. Cryst. 40 (2007), pp. 684–693.

[9] R. Frahm, M. Richwin, and D. Lützenkirchen-Hecht, *Recent advances and new applications of time-resolved X-ray absorption spectroscopy*, Phys. Scrypta T115 (2005), pp. 974–976.

[10] S. Belin, V. Briois, A. Traverse, M. Idir, and T. Moreno, *Samba: a new beamline at SOLEIL for X-ray Absorption Spectroscopy in the 4-40 keV energy range*, Phys. Scrypta T115 (2005), pp. 980–983.

[11] E. Guilminot, D. Neff, C. Rémazeilles, S. Réguer, F. Mirambet, P. Dillmann, P. Refait, N. Huet, F. Nicot, F. Mielcarek, and J. Rebière, *Etude des effets des traitements de déchloruration sur les produits de corrosion du fer par des techniques physicochimiques analytiques de pointe*, Techne Actes du colloque Science des Matériaux du patrimoine Culturel (2008), pp. 150–156.

[12] A.M. Flank, G. Cauchon, P. Lagarde, S. Bac, M. Janousch, R. Wetter, J.M. Dubuisson, M. Idir, F. Langlois, T. Moreno, and D. Vantelon, *LUCIA, a microfocus soft XAS beamline*, Nucl. Inst. Meth. In Phys. Res. B 246 (2006), pp. 269–274.

[13] B. Ravel and M. Newville, *ATHENA, ARTEMIS, HEPHAESTUS: data analysis for X-ray absorption spectroscopy using IFEFFIT*, J. Synch. Rad. 12 (2005), pp. 537–541.

[14] J.B. Parise and B.G. Hyde, *The structure of atacamite and its relationship to spinel*, Acta Cryst. C42 (1986), pp. 1277–1280.

[15] E. Berrier, S. Cristol, and X. Secordel (manuscript in preparation).

[16] B. Krebs, A. Müller, and H.H. Beyer, *The crystal structure of rhenium(VI) oxide*, Inorg. Chem. 8 (1969), pp. 436–443.

[17] H. Beyer, O. Glemser, and B. Krebs, *Dirheniumdihydratoheptoxid $Re_2O_7(OH_2)_2$ – ein neuer type von wasserbindung in einem aquoxid*, Angew. Chem. 80 (1968), pp. 286–287.

[18] J.G. Mesu, A.M. Beale, F.M.F. de Groot, and B. Weckhuysen, *Probing of influence of X-rays on aqueous copper solutions using time-resolved in situ combined video/X-ray absorption near edge/ultraviolet-visible spectroscopy*, J. Phys. Chem. B 110 (2006), pp. 17671–17677.

[19] S. Reguer, P. Dillmann, and F. Mirambet, *Buried iron archaeological artefacts: corrosion mechanisms related to the presence of Cl-containing phases*, Corrosion Sci. 49 (2007), pp. 2726–2744.

[20] S. Reguer, D. Neff, L. Bellot-Gurlet, and P. Dillmann, *Deterioration of iron archaeological artefacts: micro-Raman investigation on Cl-containing corrosion products*, J. Synch. Rad 38 (2007), pp. 389–397.

[21] M. Taillefumier, D. Cabaret, A.-M. Flank, and F. Mauri, *X-ray absorption near-edge structure calculations with the pseudopotentials: Application to the K edge in diamond and alpha-quartz*, Phys. Rev. B. 66 (2002), p. 195107 (8 pages).